Supplementary

Table S1. Sequences in the master alignment. The alignment comprises 22 sequences, 12 kinetoplastid and 10 mammalian, numbered in the frame of the *L. infantum* sequence across 425 columns, and was built by adding the 13 non-*Leishmania* sequences to the nine-species *Leishmania* alignment with MAFFT under --add --keep length so that reference columns are preserved. All alignment-derived values reported in the manuscript derive from this single alignment. Leishmania sequences are identified by TriTrypDB gene identifier and the remainder by UniProt accession. Identity is to the *L. infantum* reference and is computed over positions where both sequences have a residue, so it describes the shared region rather than the full length of the longer sequence. The nine Leishmania sequences are all 425 residues and ungapped, so for those the two are the same. Pairwise identity and similarity among the nine Leishmania orthologues are given in Table S2.

No annotated NTPDase family member was available for *T. congolense*, *T. vivax* or *C. fasciculata*, which bounds the kinetoplastid survey at three species beyond Leishmania.

Group	Species	Identifier	Source	Length (aa)	Identity to *L. infantum* (%)
Leishmania	*Leishmania infantum JPCM5*	LINF_150005200	TriTrypDB	425	—
Leishmania	*Leishmania donovani BPK282A1*	LdBPK_150030.1	TriTrypDB	425	99.8
Leishmania	*Leishmania major Friedlin*	LmjF.15.0030	TriTrypDB	425	92.0
Leishmania	*Leishmania tropica L590*	LTRL590_150005200.1	TriTrypDB	425	95.3
Leishmania	*Leishmania aethiopica L147*	LAEL147_000207800.1	TriTrypDB	425	95.3
Leishmania	*Leishmania mexicana*	LmxM.15.0030.1	TriTrypDB	425	88.2
Leishmania	*Leishmania amazonensis*	LAMA_000225600	TriTrypDB	425	88.0
Leishmania	*Leishmania braziliensis*	LbrM.15.0030	TriTrypDB	425	79.3
Leishmania	*Leishmania panamensis*	LPAL13_150005200	TriTrypDB	425	80.5
Other kinetoplastid	*Trypanosoma brucei*	Q6IEK0	UniProt	603	36.3
Other kinetoplastid	*Trypanosoma cruzi*	Q6QHT8	UniProt	636	37.9
Other kinetoplastid	*Bodo saltans*	A0A0S4IR76	UniProt	573	38.8
Human	*Homo sapiens ENTPD1*	P49961	UniProt	510	30.5
Human	*Homo sapiens ENTPD2*	Q9Y5L3	UniProt	495	33.2
Human	*Homo sapiens ENTPD3*	O75355	UniProt	529	31.6
Human	*Homo sapiens ENTPD4*	Q9Y227	UniProt	616	29.5
Human	*Homo sapiens ENTPD5*	O75356	UniProt	428	32.9
Human	*Homo sapiens ENTPD6*	O75354	UniProt	484	32.0
Human	*Homo sapiens ENTPD7*	Q9NQZ7	UniProt	604	32.4
Human	*Homo sapiens ENTPD8*	Q5MY95	UniProt	495	30.7
Rodent	*Rattus norvegicus NTPDase1*	P97687	UniProt	511	31.6
Rodent	*Rattus norvegicus NTPDase2*	O35795	UniProt	495	32.0

Table S2. Pairwise sequence conservation metrics for NTPDase1 across nine *Leishmania* orthologs, calculated across all 36 pairwise combinations using the SIAS web server. Pairwise identity and similarity are expressed as percentages; global similarity is a normalized score between 0 and 1.

Metric	Mean	Min	Max	SD
Pairwise identity (%)	87.43	77.88	99.76	6.74
Pairwise similarity (%)	91.17	81.88	100.00	5.99
Global similarity	0.878	0.780	0.990	0.064

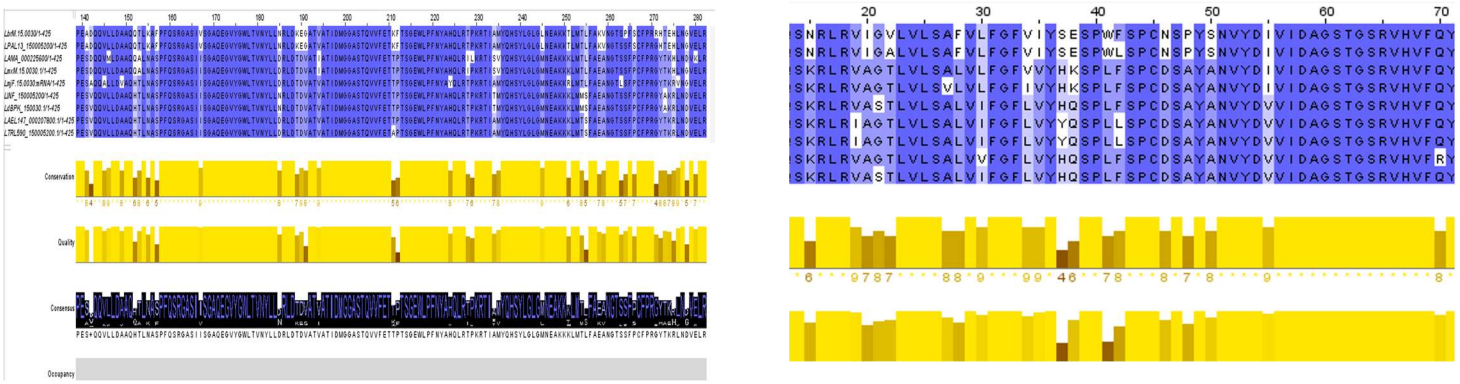


Figure S1. Multiple sequence alignment and conservation analysis of NTPDase1 across nine *Leishmania* species. (a) Full alignment with percentage identity colouring (Jalview); (b) zoomed view of the predicted hinge region (residues 40-51) with conservation histogram highlighting the conserved segment selected for mutational analysis.

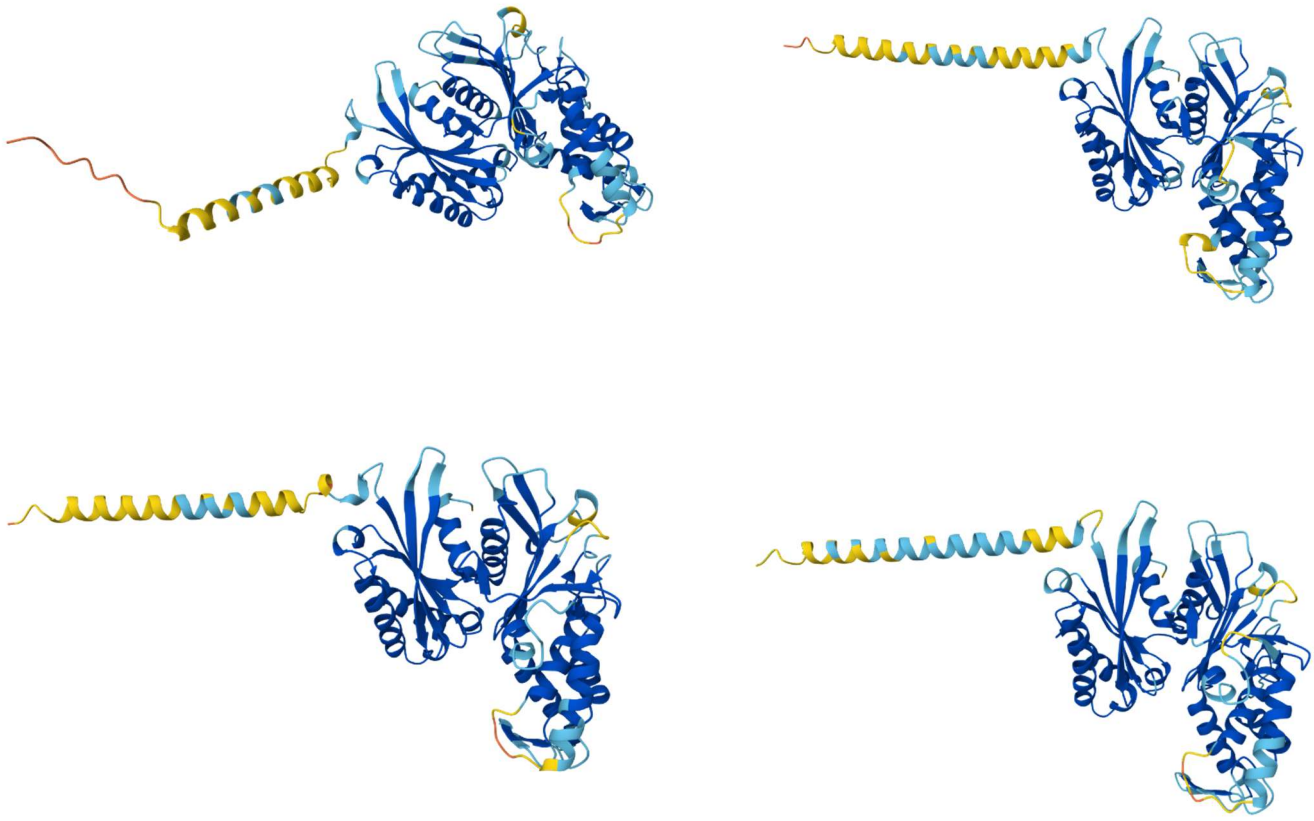


Figure S2. AlphaFold-predicted structures of wild-type and mutant *Leishmania* NTPDase1. Predicted structures are coloured according to per-residue pLDDT confidence scores, with darker blue indicating higher confidence and yellow/orange indicating lower confidence. The top row shows *L. major* WT (left) and mutant (right), while the bottom row shows *L. infantum* WT (left) and mutant (right). Mutant models contain the Pro40Ala, Ser43Ala, Pro44Ala and Tyr49Phe substitutions.

Table S3. Backbone deviation between the predicted wild-type and mutant models, by region. Values are Cα root-mean-square deviation after superposition on the catalytic core. Deviation is confined almost entirely to the N-terminal region, which was not included in the simulated construct.

Region	Residues	*L. infantum* (Å)	*L. major* (Å)
Catalytic core	52 to 425	0.74	0.93
Hinge segment	40 to 51	3.05	2.47
Transmembrane segment	20 to 35	13.5	18.7

Table S4. Per-replicate linear slopes of catalytic-core Cα RMSD, tested against zero in each analysis window. Slopes were fitted to each trajectory separately after superposition on residues 52 to 425, and the mean is taken across the ten replicates of each arm. All twelve system-window combinations have a positive mean slope and eleven of the twelve are significantly greater than zero, the exception being the *L. infantum* mutant in the 30 to 55 ns window. Three of the four systems are therefore still drifting across the final 25 ns, and the core is not presented as having reached a stationary value. p values are two-tailed one-sample t tests of the ten per-replicate slopes against zero.

Window	System	Mean slope (Å ns^{-1})	SD	p vs zero	n
5 to 30 ns	*L. infantum* wild type	0.0657	0.0550	0.0044	10
5 to 30 ns	*L. infantum* mutant	0.0615	0.0500	0.0037	10
5 to 30 ns	*L. major* wild type	0.0263	0.0348	0.0405	10
5 to 30 ns	*L. major* mutant	0.0582	0.0528	0.0069	10
30 to 55 ns	*L. infantum* wild type	0.0381	0.0508	0.0420	10
30 to 55 ns	*L. infantum* mutant	0.0152	0.0382	0.2418	10
30 to 55 ns	*L. major* wild type	0.0188	0.0198	0.0149	10
30 to 55 ns	*L. major* mutant	0.0133	0.0134	0.0120	10
5 to 55 ns	*L. infantum* wild type	0.0530	0.0223	<0.0001	10
5 to 55 ns	*L. infantum* mutant	0.0432	0.0218	0.0001	10
5 to 55 ns	*L. major* wild type	0.0187	0.0198	0.0150	10
5 to 55 ns	*L. major* mutant	0.0273	0.0197	0.0017	10

Table S5. Catalytic-core RMSD drift rate compared between genotypes. Each test is a two-tailed Welch test on ten per-replicate slopes per arm. Drift rate does not differ between genotypes in either species in any window, at p = 0.1317 to 0.8581 across the six tests, so the drift affects the absolute magnitude of core deviation and not the comparison between arms. Difference is mutant minus wild type. Positive values indicate faster drift in the mutant.

Window	Species	Wild type (Å ns⁻¹)	Mutant (Å ns⁻¹)	Difference	p
5 to 30 ns	*L. infantum*	0.0657	0.0615	-0.0043	0.8581
5 to 30 ns	*L. major*	0.0263	0.0582	0.0318	0.1317
30 to 55 ns	*L. infantum*	0.0381	0.0152	-0.0229	0.2709
30 to 55 ns	*L. major*	0.0188	0.0133	-0.0056	0.4716
5 to 55 ns	*L. infantum*	0.0530	0.0432	-0.0099	0.3309
5 to 55 ns	*L. major*	0.0187	0.0273	0.0086	0.3415

Table S6. Cβ-Sγ-Sγ-Cβ dihedral of the Cys45-Cys124 disulfide, compared between genotypes in each analysis window. The dihedral was computed per frame from the four atoms and averaged within each window for every trajectory, giving ten values per arm. It is negative throughout, around -78 to -82 degrees, and is reported here as a magnitude so that an increase corresponds to a larger torsion. All p values are two-tailed Welch tests on ten per-replicate values per arm. Per-replicate values are given in the deposited data.

Window	Species	Wild type (deg)	Mutant (deg)	Difference (deg)	Hedges g	p
5 to 30 ns	*L. infantum*	78.52	80.24	+1.719	+1.12	0.0221
5 to 30 ns	*L. major*	82.29	80.49	−1.798		0.5587
30 to 55 ns	*L. infantum*	78.68	81.23	+2.545	+1.70	0.0019
30 to 55 ns	*L. major*	82.59	81.28	−1.310		0.6854
5 to 55 ns	*L. infantum*	78.60	80.73	+2.132	+1.49	0.0049
5 to 55 ns	*L. major*	82.44	80.89	−1.554		0.6141

Post-hoc measures, reported without multiple-comparison correction, and no part of the proposed mechanism rests on them. The sulfur-sulfur distance is constrained by the covalent bond and does not differ between genotypes. In *L. major*, wild-type replicate 3 is an outlier, averaging 106.0 degrees across its full production trajectory against a range of 77.7 to 82.3 in the other nine, which raises that arm's standard deviation from 1.40 to 8.51. Excluding it, the *L. major* difference is +1.48 degrees at p = 0.0182, the same direction as *L. infantum* rather than the opposite one. The null result in that species therefore rests on a single trajectory and is reported as uninformative rather than as evidence of no effect.

Table S7. Site-directed mutagenesis primers for the hinge substitutions. Primers are designed for back-to-back, whole-plasmid amplification with Q5 polymerase following the design rules of NEBaseChanger (New England Biolabs), against the native coding sequence of each species as deposited in TriTrypDB (LINF_150005200 and LmjF.15.0030). Mutated bases are shown in upper case and lower case letters denotes template-matching annealing sequences. The four target codons occupy bases 118 to 147 of the coding sequence, too wide a span for a single mutagenic primer, so the quadruple variant is constructed in two sequential rounds. The step 1 pair introduces P40A, S43A and P44A together and the step 2 pair introduces Y49F on the step 1 product. The step 2 pair also serves as the single-mutant pair for Y49F. Pairs for the remaining three single substitutions are given separately to allow the contribution of each residue to be isolated. Tm is the predicted melting temperature of the primer as synthesised, by the nearest-neighbour method at 50 mM monovalent salt and 2 mM magnesium.

Species	Target	Primer	Sequence (5′ to 3′)	Length (nt)	Tm (°C)
L. infantum	P40A, S43A, P44A (step 1)	Forward	ctatcaaagcGctctgctcGccGcatgtgactc	33	74
L. infantum	P40A, S43A, P44A (step 1)	Reverse	taaacgaggaaaccgaagataacaagcgcg	30	68
L. infantum	Y49F (step 2)	Forward	gactcggcgTcgcgaatgtatac	24	65
L. infantum	Y49F (step 2)	Reverse	acatggggagagcagagggc	20	66
L. infantum	P40A	Forward	ctatcaaagcGctctgctctccc	23	64
L. infantum	P40A	Reverse	taaacgaggaaaccgaagataacaagcg	28	64
L. infantum	S43A	Forward	ccctctgctcGccccatgtgac	22	69
L. infantum	S43A	Reverse	ctttgatagtaaacgaggaaaccgaagat	29	62
L. infantum	P44A	Forward	ctctgctctccGcatgtgactc	22	64
L. infantum	P44A	Reverse	ggctttgatagtaaacgaggaaaccgaag	29	65
L. major	P40A, S43A, P44A (step 1)	Forward	ccatcaaagcGctttgttcGccGcatgtgactc	33	74
L. major	P40A, S43A, P44A (step 1)	Reverse	tagacgaggaaaccgaagataacaagcgcg	30	69
L. major	Y49F (step 2)	Forward	gactcggcgTcgcgaatgtatac	24	65
L. major	Y49F (step 2)	Reverse	acatggggagaacaaagggctttg	24	65
L. major	P40A	Forward	tctaccatcaaagcGctttgttctcc	26	64
L. major	P40A	Reverse	cgaggaaaccgaagataacaagcgc	25	65
L. major	S43A	Forward	ccctttgttcGccccatgtgac	22	65
L. major	S43A	Reverse	ctttgatggtagacgaggaaaccgaag	27	64
L. major	P44A	Forward	tttgttctccGcatgtgactcgg	23	64
L. major	P44A	Reverse	gggctttgatggtagacgaggaaac	25	64

These primers are provided as a proposed experimental resource for future validation. They have not been synthesised or tested, and no claim is made here that any construct has been generated. Predicted melting temperatures should be confirmed in NEBaseChanger before synthesis, as that tool treats mismatched bases differently when setting the annealing temperature. GC content ranges from 38 to 68 per cent across the twenty primers.

Table S8. Species-by-condition interaction for five geometric measures. The interaction is the direct contrast of the two condition effects, that is the *L. major* effect minus the *L. infantum* effect, with its standard error. A significant interaction would establish that the two species respond differently. None of the five is established, at p = 0.1021 to 0.7419, so a result that reaches significance in one species and not the other is not evidence of a difference between them.

Measure	*L. infantum* effect (deg)	*L. major* effect (deg)	Interaction (deg)	SE	p
Elbow angle, as published	+5.12	+15.71	+10.59	6.48	0.1021
Elbow angle, origin Cα 40	+5.57	+7.49	+1.92	5.82	0.7419
Terminal-free hinge axis	+13.12	+7.70	-5.42	4.19	0.1956
P3 hinge angle (pre-registered)	+9.35	+4.79	-4.56	6.65	0.4930
P3 mean-vector angle	+9.19	+3.37	-5.82	7.15	0.4157

All tests are two-sided. Effects are mutant minus wild type in the primary 5 to 30 ns window. The species-specific pattern described in the Results is therefore reported as a description of each species separately rather than as a demonstrated dissociation between them.

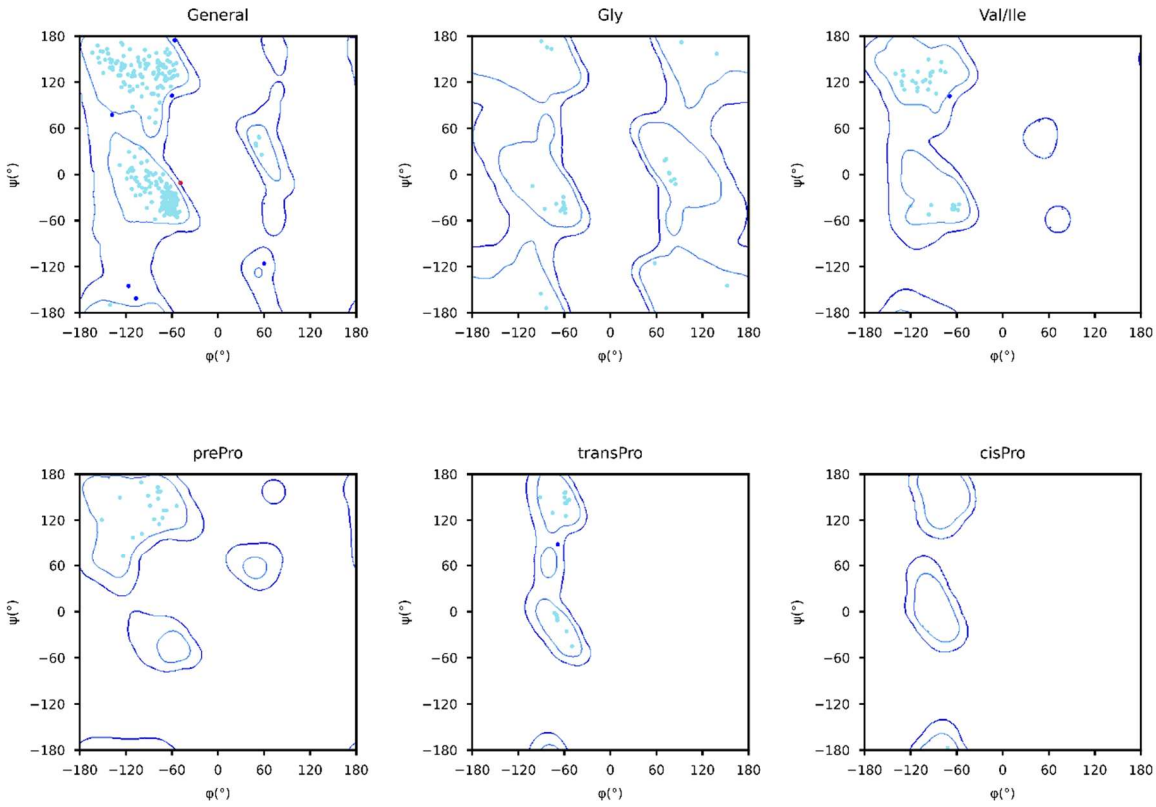
Minimum detectable interactions, computed at 80 per cent power two-sided at alpha 0.05 from the standard errors above, are 18.7, 16.8, 12.1, 19.1 and 20.6 degrees in the order listed. The interaction test is therefore less sensitive than the single-species comparisons it contrasts, and failure to establish an interaction does not establish equivalence.

Table S9. Per-replicate drift slopes of the terminal-free hinge axis across the full 5 to 55 ns window. A linear slope was fitted to the axis angle against time within each trajectory, giving ten slopes per arm. No arm has a mean slope that differs from zero, so the genotype difference in axis angle is not attributable to a difference in drift rate between the two arms.

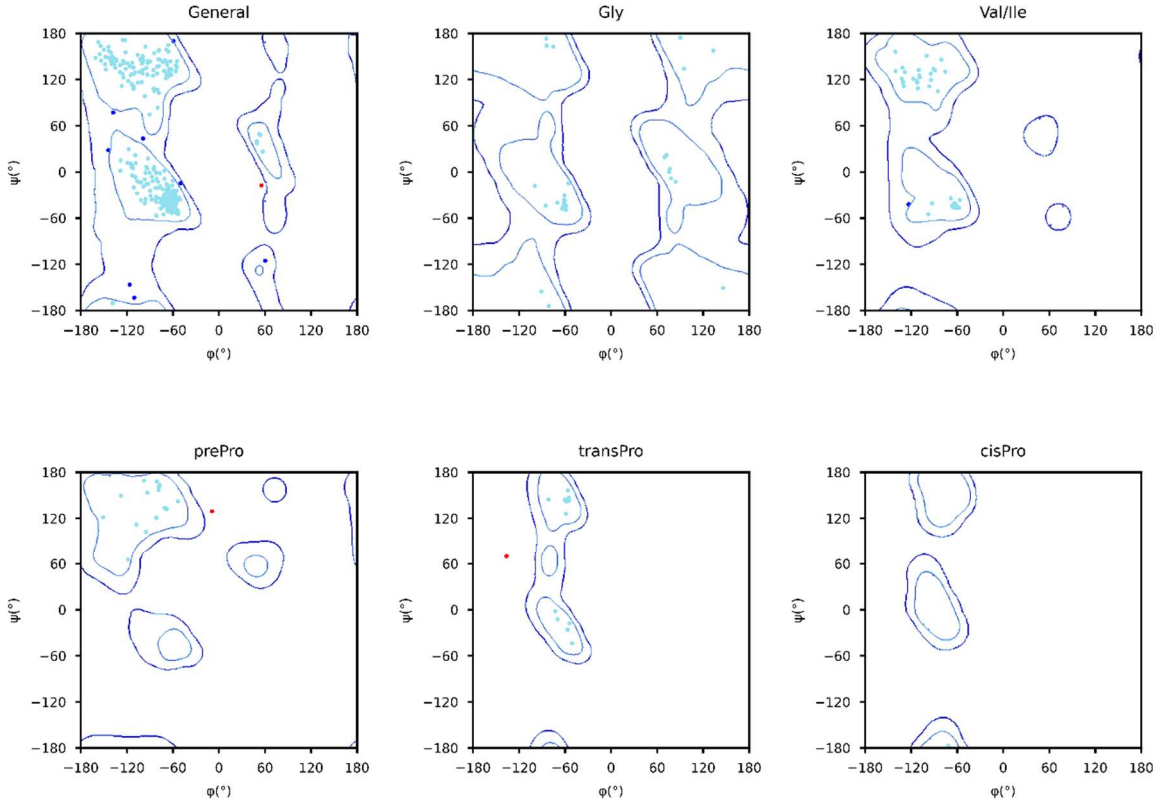
Replicate	*L. infantum* wild type	*L. infantum* mutant	*L. major* wild type	*L. major* mutant
1	-0.098	0.104	0.410	0.328
2	-0.190	-0.279	-0.185	-0.125
3	-0.064	-0.163	-0.180	-0.177
4	-0.117	-0.407	-0.448	0.109
5	-0.275	0.135	0.032	-0.024
6	-0.028	-0.201	0.012	-0.472
7	0.084	0.135	-0.069	0.366
8	-0.245	-0.016	-0.187	0.014
9	0.184	-0.069	-0.020	-0.125
10	-0.397	0.010	-0.797	0.605
Mean ± SD	-0.114 ± 0.172	-0.075 ± 0.184	-0.143 ± 0.317	+0.050 ± 0.313
p vs zero	0.0651	0.2298	0.1874	0.6265

p values are two-tailed one-sample t tests of the ten per-replicate slopes against zero. The genotype difference in slope is +0.039 deg ns^{-1} in *L. infantum* (p = 0.6284) and +0.193 in *L. major* (p = 0.1876), as reported in Supplementary Table S23.

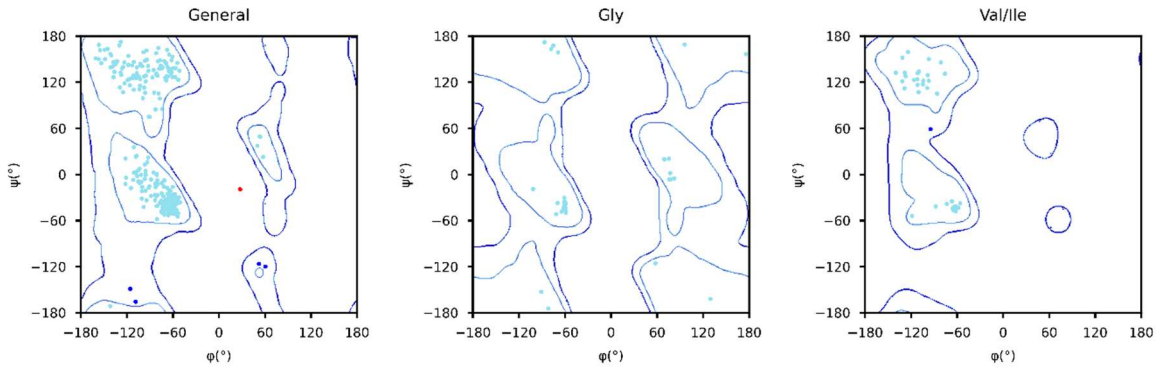
A

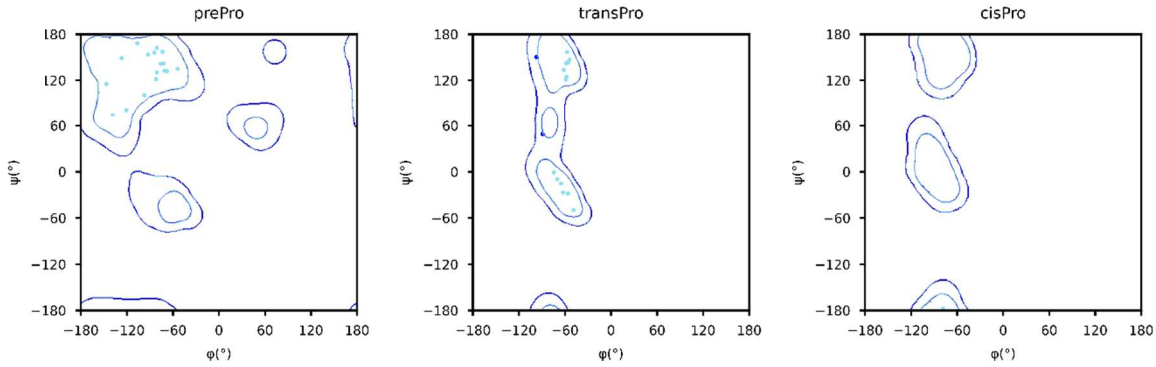

General
Gly
Val/Ile
prePro
transPro
cisPro
ψ(°)
φ(°)
180
120
60
0
−60
−120
−180

B

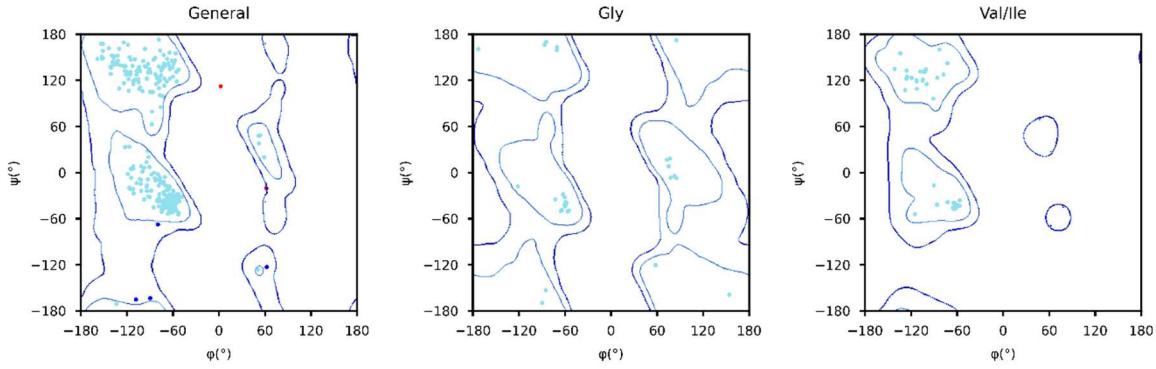

General
Gly
Val/Ile
prePro
transPro
cisPro
ψ(°)
φ(°)
180
120
60
0
−60
−120
−180

C


General
Gly
Val/Ile
ψ(°)
φ(°)
180
120
60
0
−60
−120
−180


prePro
transPro
cisPro
ψ(°)
φ(°)
180
120
60
0
−60
−120
−180

D


General
Gly
Val/Ile
ψ(°)
φ(°)
180
120
60
0
−60
−120
−180

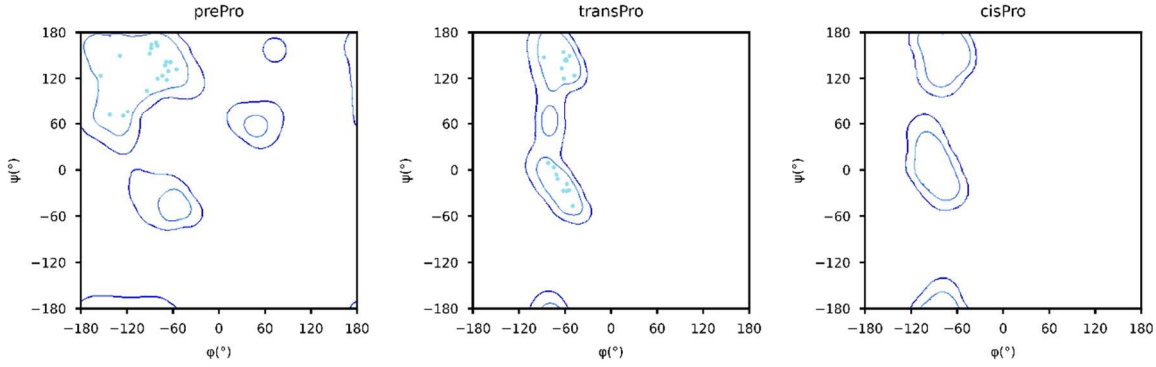

prePro
transPro
cisPro
ψ(°)
φ(°)
180
120
60
0
−60
−120
−180

Figure S3. Ramachandran plots for the four predicted NTPDase1 models, generated with the RamPlot web server [36] from backbone φ and ψ torsion angles. (a) *L. major* wild type, 97.9 per cent of residues favoured, 1.9 per cent allowed and 0.2 per cent disallowed, the single disallowed residue being Arg324. (b) *L. infantum* wild type, 97.9, 1.7 and 0.5 per cent, with Thr302 and Arg324 disallowed. (c) *L. major* hinge mutant, 97.2, 2.4 and 0.5 per cent, with Arg2 and Lys343 disallowed. (d) *L. infantum* hinge mutant, 98.4, 1.4 and 0.2 per cent, with Arg324 disallowed. Across the four models 97.8 per cent of residues are in favoured regions, 1.8 per cent allowed and 0.4 per cent disallowed. No disallowed residue falls within the hinge segment, residues 36 to 51.

Supplementary Methods: codon-level selection analysis. Coding sequences for the nine Leishmania orthologues were retrieved from TriTrypDB and back-translated onto the protein alignment described in Section 2.1 to give an in-frame codon alignment. That alignment is ungapped across 425 columns, so the correspondence between codon and residue number is one to one and the numbering of the reference sequence is preserved. Each coding sequence was verified to translate exactly to its aligned protein sequence before analysis. A neighbour-joining tree was inferred from the protein alignment and rooted at the midpoint, recovering a topology consistent with the accepted phylogeny of the genus, with the two Viannia species basal. Branch lengths were re-estimated under the codon model rather than taken from this tree. Site-level selection was assessed in HyPhy v2.5.104 under the MG94xREV codon model using two independent methods, fixed-effects likelihood (FEL) and the Bayesian method FUBAR. A site was called as under purifying selection when FEL returned $p < 0.05$ with dN below dS, or when the FUBAR posterior probability that dS exceeds dN exceeded 0.9. Enrichment of the hinge segment relative to the remainder of the gene was tested by two-tailed Fisher exact test on the counts of sites meeting the FEL criterion. HyPhy is described in Kosakovsky Pond, Poon, Velazquez et al., Molecular Biology and Evolution 2020, 37, 295-299.

Table S10. Site-level selection across the hinge segment, residues 40 to 51, from the nine-orthologue codon alignment. dS and dN are FEL maximum-likelihood rate estimates, and FEL p is the two-tailed likelihood-ratio p value for dN differing from dS. The FUBAR column gives the posterior probability that dS exceeds dN. Seven of the twelve positions are invariant across the nine orthologues. None of the four substituted positions reaches significance by either method, and positions 40 and 49 carry no substitutions of any kind, synonymous included. Across the whole gene the fitted non-synonymous to synonymous rate ratio was 0.265, and 174 of 425 codons (40.9%) carry no substitutions. The segment is not enriched for sites meeting the FEL criterion relative to the remainder of the gene, at 1 of 12 against 38 of 413 (Fisher exact p = 1.0). The single position in the segment reaching significance is Asn51, which is not among those substituted.

Position	Residue	Invariant	dS	dN	FEL p	FUBAR P(dS > dN)
40[a]	Pro	Yes	0.000	0.000	1.0000	0.600
41	Leu	No	2.784	1.173	0.6105	0.685
42	Leu	No	0.000	2.010	0.3306	0.272
43[a]	Ser	Yes	1.850	0.000	0.1092	0.861
44[a]	Pro	Yes	1.546	0.000	0.1180	0.856
45[b]	Cys	Yes	1.941	0.000	0.0902	0.863
46	Asp	No	0.010	0.568	0.6018	0.474

47	Ser	Yes	0.000	0.000	1.0000	0.633
48	Ala	No	1.542	0.997	0.7509	0.662
49[a]	Tyr	Yes	0.000	0.000	1.0000	0.670
50	Ala	No	0.007	0.881	0.4022	0.402
51	Asn	Yes	9.598	0.000	0.0043	0.982

[a] Substituted in the hinge mutant. [b] Cysteine of the Cys45-Cys124 disulfide pair.

Table S11. Outlier audit across all forty trajectories. Every pre-registered and post-hoc metric was screened within each of the four arms, giving twelve metrics tested in four arms of ten replicates. Outliers were identified by the modified z score, defined as 0.6745 times the deviation from the arm median divided by the median absolute deviation of that arm, with a threshold of 3.5. Twenty-one replicate-metric combinations exceeded that threshold and are listed below. For each, the table gives the value, the median of the other replicates in that arm, the standard deviation of the arm with and without the replicate, and the two-tailed Welch p value for the genotype comparison computed with all ten replicates and with that replicate excluded. The two results on which the manuscript rests are not outlier-driven. The terminal-free axis comparison in *L. infant*um remains below p = 0.0001 with either flagged replicate removed, and the hinge helix comparison strengthens from p = 0.0038 to p = 0.0011. Several null comparisons are sensitive to exclusion and are flagged accordingly; none is a result claimed in the manuscript.

Metric	Class	Species	Arm	Replicate	Value	Arm median	Modified z	p, all ten	p, excluded
P1 core RMSF (Å)	pre-registered	*L. infantum*	WT	1	2.209	1.117	6.30	0.9868	0.2740
P2 hinge RMSF (Å)	pre-registered	*L. infantum*	WT	1	3.823	2.037	7.57	0.5145	0.1004
P2 hinge RMSF (Å)	pre-registered	*L. infantum*	MUT	7	3.668	2.220	5.26	0.5145	0.8807
P3 hinge angle (deg)	pre-registered	*L. infantum*	MUT	1	40.601	26.520	5.89	0.0014	0.0020
P3 hinge angle (deg)	pre-registered	*L. major*	WT	3	60.017	23.706	3.98	0.4486	0.1326
P4 active-site spread (Å)	pre-registered	*L. infantum*	WT	2	25.229	20.484	3.80	0.4929	0.0624
Terminal-free axis (deg)	post-hoc	*L. infantum*	MUT	1	51.523	43.043	3.82	<0.0001	<0.0001
Terminal-free axis (deg)	post-hoc	*L. infantum*	MUT	5	54.605	43.043	5.20	<0.0001	<0.0001
Elbow angle from Ca36 (deg)	post-hoc	*L. infantum*	MUT	1	47.028	15.860	6.19	0.2749	0.5497
Elbow angle from Ca36 (deg)	post-hoc	*L. infantum*	MUT	5	42.583	15.860	5.31	0.2749	0.5123
P3 mean-vector angle (deg)	post-hoc	*L. infantum*	MUT	1	39.465	24.124	5.74	0.0027	0.0035
P3 mean-vector angle (deg)	post-hoc	*L. major*	WT	3	59.076	21.372	3.58	0.6176	0.2361

P3 order parameter S	post-hoc	L. infantum	WT	1	0.937	0.985	-15.33	0.2571	0.0280
P3 order parameter S	post-hoc	L. infantum	WT	9	0.969	0.985	-5.09	0.2571	0.2384
P3 order parameter S	post-hoc	L. infantum	WT	10	0.962	0.985	-7.31	0.2571	0.1898
P3 order parameter S	post-hoc	L. infantum	MUT	7	0.938	0.970	-4.26	0.2571	0.4722
Disulfide chi3 (deg)	post-hoc	L. infantum	MUT	1	-75.187	-80.993	10.49	0.0213	<0.0001
Disulfide chi3 (deg)	post-hoc	L. major	WT	3	-108.422	-79.076	-61.27	0.5665	0.1399
Disulfide chi3 (deg)	post-hoc	L. major	WT	4	-83.545	-79.076	-9.33	0.5665	0.6368
Disulfide chi3 (deg)	post-hoc	L. major	WT	7	-76.955	-79.076	4.43	0.5665	0.4892
Hinge helix occupancy (%)	post-hoc	L. infantum	MUT	5	82.520	22.020	3.51	0.0038	0.0011

L. infantum wild-type replicate 1 is flagged on three metrics and is therefore an atypical trajectory rather than a single atypical value. *L. major* wild-type replicate 3 is flagged on the disulfide dihedral at a modified z of -61.3, and its exclusion reduces the standard deviation of that arm from 9.34 to 1.74 degrees, as reported in the Results. Welch tests are two-tailed on per-replicate values, with the opposing arm held at ten replicates throughout.

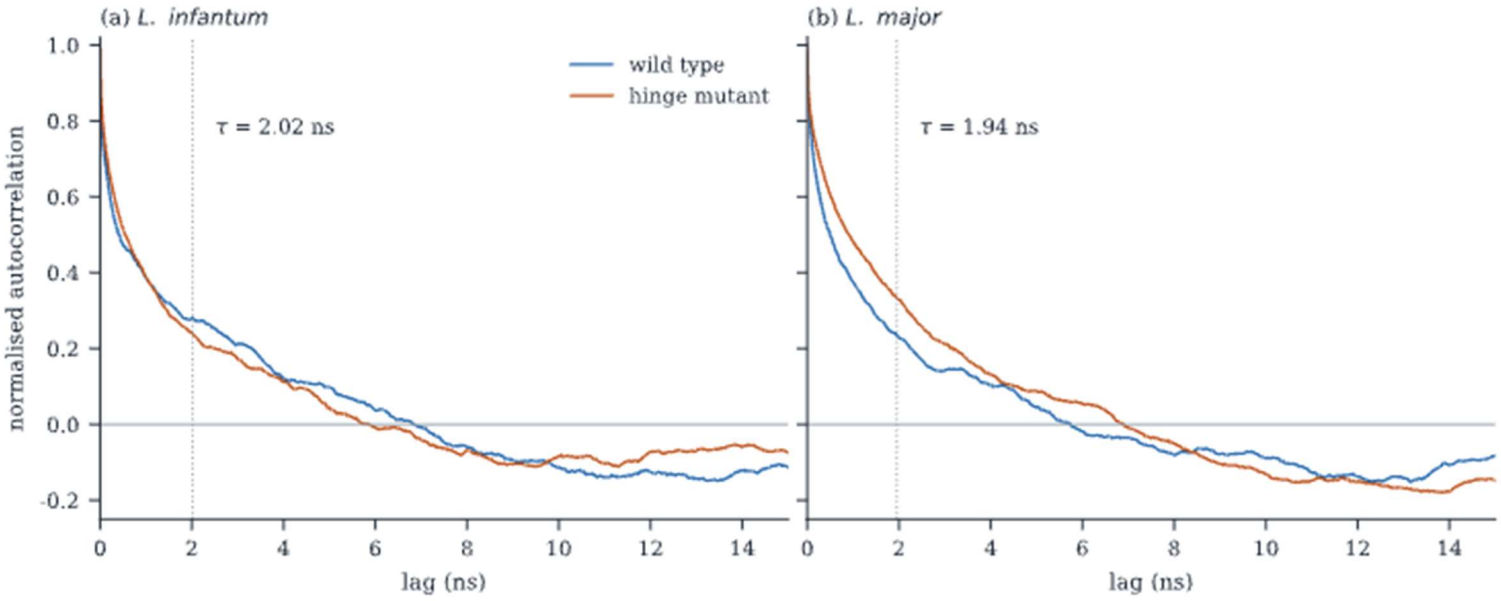


Figure S4. Autocorrelation of the terminal-free hinge axis. Normalised autocorrelation of the per-frame axis angle, averaged across the ten replicates of each arm, for (a) *L. infantum* and (b) *L. major* Wild type in blue, hinge mutant in orange. Series were linearly detrended within each replicate before the autocorrelation was computed, since the undetrended series carries the drift described in Section 3.4. The dotted vertical line marks the mean detrended integrated autocorrelation time for that species. Pooled across the four arms the integrated autocorrelation time is 1.98 ns after detrending, 3.23 ns by Sokal windowing and 4.82 ns by first zero crossing, corresponding to 6.3, 3.9

and 2.6 effectively independent samples per 25 ns analysis window. The equivalent values for the pre-registered hinge angle are 1.86, 3.31 and 5.79 ns.

Table S12. Predicted pKa values for ionisable residues lining the catalytic site. Values were calculated with PROPKA 3 on the predicted structures of each system. The residues listed are the aspartate, glutamate and histidine residues within 4.5 Å of any heavy atom of the structurally mapped active site, identified as described in Section 2.9. Model pKa is the reference value for the isolated residue. The final column gives the percentage of each residue predicted to be in the state assigned during system preparation at pH 7.4, that is deprotonated for aspartate and glutamate and neutral for histidine, taken across the four systems. Four of the five residues are assigned unambiguously. Glu172 is the exception and is discussed in the text.

Residue	Shell	Model pKa	*L. infantum* WT	*L. infantum* mutant	*L. major* WT	*L. major* mutant	% in assigned state at pH 7.4
Asp58	4.5 Å	3.80	4.02	5.19	5.36	5.34	99 to 100
His67	4.5 Å	6.50	6.59	6.71	6.67	6.62	83 to 87
Glu89	4.5 Å	4.50	3.91	4.21	4.22	4.20	approximately 100
Glu172	4.5 Å	4.50	7.26	7.16	7.10	7.21	58 to 67
Glu247	4.5 Å	4.50	5.01	4.93	4.76	4.87	approximately 100

Calculations were performed on apo structures containing no bound nucleotide and no divalent cation. A coordinated magnesium ion would be expected to lower the pKa of a proximal carboxylate, so these values are likely to overestimate the holo-state pKa of the acidic residues. PROPKA operates on a single static conformation and does not sample the conformational ensemble explored during simulation. Glu172 lines the site but is not among the six structurally mapped active-site residues.

Table S13. Screw-axis decomposition of the reorientation of the catalytic core relative to the hinge. Each frame was superposed on the hinge CA atoms, residues 40 to 51, and the residual motion of the catalytic core was decomposed into a rotation about a screw axis and a translation along that same axis. Means and standard deviations are taken across the ten replicates of each arm. Inference is at the level of the trajectory, by Welch t test on the ten replicate means per arm, with Holm correction applied across the four species-by-window comparisons within each component. The lever arm is repeated from Section 3.6 so that the three quantities can be read together. A translation that is not zero is what distinguishes this motion from a rotation about a stationary pivot. These analyses were added at revision and were not pre-registered. Values were calculated from the pair-replicate data.

Species	Window	Wild type mean	Wild type SD	Hinge mutant mean	Hinge mutant SD	Difference	Hedges' g	p	Holm p
Rotation about the screw axis (deg)									
L. infantum	5 to 30 ns	24.532	7.458	29.791	17.344	+5.26	+0.38	0.3953	0.8974
L. infantum	30 to 55 ns	34.539	8.946	28.919	13.910	-5.62	-0.46	0.2991	0.8974
L. major	5 to 30 ns	19.588	6.035	37.060	11.386	+17.47	+1.84	0.0008	0.0032
L. major	30 to 55 ns	28.529	11.110	34.722	15.708	+6.19	+0.44	0.3237	0.8974
Translation along the screw axis (Å)									
L. infantum	5 to 30 ns	-0.458	0.587	0.460	1.513	+0.92	+0.77	0.0998	0.2993
L. infantum	30 to 55 ns	-1.479	1.378	1.148	1.571	+2.63	+1.70	0.0009	0.0036
L. major	5 to 30 ns	1.157	1.098	0.731	0.800	-0.43	-0.42	0.3358	0.5590
L. major	30 to 55 ns	1.407	1.053	1.971	1.205	+0.56	+0.48	0.2795	0.5590
Lever arm, hinge to core centroid (Å)									
L. infantum	5 to 30 ns	40.809	0.982	39.643	1.391	-1.17	-0.93	0.0456	0.0737
L. infantum	30 to 55 ns	41.648	1.467	39.895	0.631	-1.75	-1.49	0.0045	0.0180
L. major	5 to 30 ns	43.361	1.193	41.574	2.111	-1.79	-1.00	0.0350	0.0737
L. major	30 to 55 ns	42.969	2.117	40.853	1.702	-2.12	-1.06	0.0246	0.0737

Holm correction is applied within each component across its four species-by-window comparisons, not across all twelve.

Table S14. Inter-lobe geometry measured without the 90-degree ceiling. The published inter-lobe cleft angle is the acute angle between two undirected principal axes, so it cannot exceed 90 degrees, and any wider geometry is folded back below it. Two measures free of that ceiling were computed on the same frames. The directed angle fixes the sign of each lobe axis so that it points away from the opposite lobe, giving the full 0-to-180-degree range. The lobe centre-of-mass distance uses no angular convention at all. The acute measure is repeated for comparison. Inference is at the level of the trajectory, by Welch t test on the ten replicate means per arm, with Holm correction across the four species-by-window comparisons within each measure. The lower table gives the extent of the censoring itself. These analyses were added at revision and were not pre-registered.

Species	Window	Wild type mean	Wild type SD	Hinge mutant mean	Hinge mutant SD	Difference	Hedges' g	p	Holm p
Lobe centre-of-mass distance (Å)									
L. infantum	5 to 30 ns	24.937	1.012	24.967	0.827	+0.03	+0.03	0.9429	0.9429
L. infantum	30 to 55 ns	26.733	0.809	26.484	0.775	-0.25	-0.30	0.4906	1.0000
L. major	5 to 30 ns	25.052	1.336	24.946	1.348	-0.11	-0.08	0.8614	1.0000
L. major	30 to 55 ns	25.546	1.475	25.804	1.406	+0.26	+0.17	0.6936	1.0000
Inter-lobe angle, directed, 0 to 180 deg									
L. infantum	5 to 30 ns	74.778	4.763	74.749	4.036	-0.03	-0.01	0.9886	0.9886
L. infantum	30 to 55 ns	82.933	4.605	82.219	4.670	-0.71	-0.15	0.7349	1.0000
L. major	5 to 30 ns	74.409	6.005	74.856	6.372	+0.45	+0.07	0.8737	1.0000
L. major	30 to 55 ns	76.802	6.753	78.722	6.765	+1.92	+0.27	0.5333	1.0000
Inter-lobe angle, acute, as published (deg)									
L. infantum	5 to 30 ns	74.589	4.662	74.696	3.986	+0.11	+0.02	0.9569	1.0000
L. infantum	30 to 55 ns	81.882	3.106	81.806	4.248	-0.08	-0.02	0.9640	0.9640
L. major	5 to 30 ns	74.402	5.992	74.815	6.355	+0.41	+0.06	0.8827	1.0000
L. major	30 to 55 ns	76.788	6.737	78.656	6.719	+1.87	+0.27	0.5424	1.0000

Extent of the censoring imposed by the 90 degree ceiling

Species	Genotype	Window	Frames above 90 deg, arm mean (%)	Frames above 90 deg, highest replicate (%)	Largest directed angle (deg)
L. infantum	Wild type	5 to 30 ns	3.20	19.92	103.71
L. infantum	Wild type	30 to 55 ns	14.84	68.40	101.21
L. infantum	Hinge mutant	5 to 30 ns	1.72	13.12	95.17
L. infantum	Hinge mutant	30 to 55 ns	10.02	34.16	99.31
L. major	Wild type	5 to 30 ns	0.33	2.88	94.50
L. major	Wild type	30 to 55 ns	0.65	3.84	93.77
L. major	Hinge mutant	5 to 30 ns	1.11	5.60	98.82
L. major	Hinge mutant	30 to 55 ns	1.80	7.20	96.53

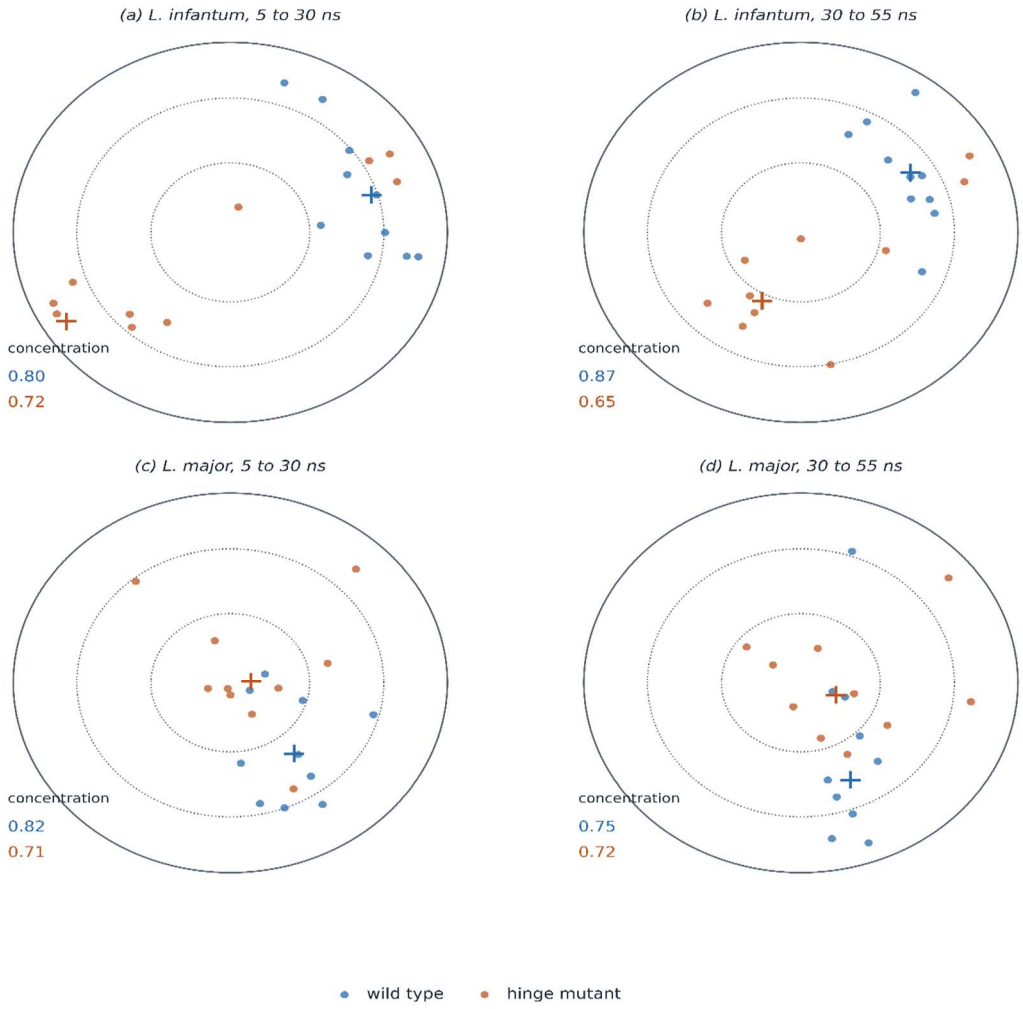


Figure S5. Principal bending axes of the hinge motion, one per replicate. Each frame was superposed on the hinge Cα atoms, residues 40 to 51, and the residual motion of the catalytic core was decomposed into a rotation about a screw axis and a translation along that axis. The rotation axis of that decomposition is the bending axis of the relative motion between the hinge and the core. Each point is one replicate, placed at its mean bending axis over the window, with ten replicates per genotype in every panel. The cross marks the mean axis of the arm. Axes are plotted on a Lambert azimuthal equal-area projection of the hemisphere. The solid circle is the equator and the dotted rings lie at 30 and 60 degrees from the viewing pole. Because an axis has no direction, each one is drawn in the hemisphere of the viewing pole, and that pole was chosen to place every observation as far from the equator as possible. This is a choice of viewpoint only and alters no angle between axes. Wild type in blue, hinge mutant in orange. The concentration printed in each panel is the principal eigenvalue of the orientation tensor for that arm. It is 1/3 for a perfectly diffuse set of axes and 1 for perfectly aligned ones, and ten isotropically distributed axes would give a median of 0.50. All eight arms exceed that null after Holm correction, so the bending occurs about a defined axis rather than representing diffuse motion of the terminus. (a,b) *L. infantum* in the 5 to 30 ns and 30 to 55 ns windows. (c,d) *L. major* in the same two windows.

Table S15. Arg65 side chain, its solvent accessibility, and its contact with Trp412. The reviewer asked whether the increase in Arg65-Trp412 contact in the *L. infantum* mutant reflects a conformational change of Arg65 or stochastic variation. Solvent accessibility is the Shrake-Rupley surface of the residue, computed on every frame with all protein atoms acting as occluders. The contact is the shortest heavy-atom distance between the two residues, and occupancy is the fraction of frames below 0.45 nm, the cutoff used in Section 3.10. Inference is at the level of the trajectory, by Welch t test on the ten replicate means per arm, with Holm correction across the four species-by-window comparisons within each measure. That is a smaller correction family than the contact screen reported in the main text, because these are targeted tests of a single pair named by the reviewer rather than a search across pairs, and they are reported as such. The lower table gives the rotamer occupancy of the two Arg65 side-chain dihedrals, computed with circular statistics. None of the 24 genotype comparisons on those occupancies approached significance, the smallest uncorrected p being 0.164, so no test statistics are tabulated for them. These analyses were added at revision and were not pre-registered. Every value is a live formula computed from the 'Per-replicate data' sheet.

Species	Window	Wild type mean	Wild type SD	Hinge mutant mean	Hinge mutant SD	Difference	Hedges' g	p	Holm p
Arg65 total solvent accessibility (nm²)									
L. infantum	5 to 30 ns	0.783	0.212	0.735	0.121	-0.048	-0.267	0.5425	1.0000
L. infantum	30 to 55 ns	0.769	0.200	0.769	0.087	-0.000	-0.003	0.9953	1.0000
L. major	5 to 30 ns	0.606	0.082	0.576	0.124	-0.030	-0.277	0.5270	1.0000
L. major	30 to 55 ns	0.607	0.095	0.585	0.150	-0.022	-0.167	0.7013	1.0000
Arg65 side-chain solvent accessibility (nm²)									
L. infantum	5 to 30 ns	0.227	0.053	0.202	0.041	-0.025	-0.517	0.2443	0.9771
L. infantum	30 to 55 ns	0.225	0.064	0.215	0.038	-0.010	-0.178	0.6834	1.0000
L. major	5 to 30 ns	0.157	0.028	0.150	0.039	-0.007	-0.192	0.6599	1.0000
L. major	30 to 55 ns	0.164	0.029	0.158	0.036	-0.006	-0.174	0.6902	1.0000
Arg65 to Trp412, shortest heavy-atom distance (nm)									
L. infantum	5 to 30 ns	0.607	0.031	0.509	0.097	-0.099	-1.312	0.0110	0.0329
L. infantum	30 to 55 ns	0.599	0.062	0.500	0.079	-0.099	-1.340	0.0061	0.0245
L. major	5 to 30 ns	0.546	0.074	0.539	0.100	-0.007	-0.082	0.8505	1.0000
L. major	30 to 55 ns	0.524	0.065	0.514	0.080	-0.010	-0.135	0.7557	1.0000
Arg65-Trp412 contact occupancy at 0.45 nm (fraction)									
L. infantum	5 to 30 ns	0.033	0.047	0.371	0.346	+0.337	+1.308	0.0131	0.0394
L. infantum	30 to 55 ns	0.061	0.138	0.384	0.304	+0.323	+1.312	0.0094	0.0375
L. major	5 to 30 ns	0.219	0.273	0.272	0.347	+0.053	+0.163	0.7085	1.0000
L. major	30 to 55 ns	0.262	0.259	0.320	0.337	+0.058	+0.186	0.6704	1.0000

Arg65 side-chain rotamer occupancy, by circular statistics

Species	Genotype	Window	chi1 g+	chi1 trans	chi1 g-	chi2 g+	chi2 trans	chi2 g-
L. infantum	Wild type	5 to 30 ns	0.508	0.041	0.451	0.154	0.730	0.116
L. infantum	Wild type	30 to 55 ns	0.659	0.100	0.241	0.062	0.793	0.145
L. infantum	Hinge mutant	5 to 30 ns	0.596	0.138	0.266	0.135	0.821	0.045
L. infantum	Hinge mutant	30 to 55 ns	0.638	0.090	0.273	0.024	0.936	0.040
L. major	Wild type	5 to 30 ns	0.422	0.014	0.564	0.147	0.709	0.144
L. major	Wild type	30 to 55 ns	0.529	0.124	0.347	0.019	0.788	0.194

L. major	Hinge mutant	5 to 30 ns	0.254	0.060	0.686	0.253	0.674	0.073
L. major	Hinge mutant	30 to 55 ns	0.465	0.036	0.499	0.066	0.844	0.090

Table S16. Structural comparison of the *Leishmania* juxtamembrane hinge against the human NTPDases. Each human AlphaFold model was superimposed on *L. infantum* NTPDase1 using the catalytic core, residues 52 to 425, with correspondence taken from a BLOSUM62 sequence alignment and refined by iterative rejection of outlying pairs. The quantity tabulated is the distance from each *L. infantum* Calpha to the nearest Calpha in the superimposed human model, so a small value means a human backbone occupies that position and a large one means none does. The upper table gives the distribution of that distance within the conserved core, which calibrates what counts as structurally equivalent. The lower table gives it residue by residue across the hinge. Positions whose smallest distance over all six models exceeds the pooled 95th percentile of the core distribution has no backbone equivalent in any human NTPDase examined. Both sides are predicted structures, and the *L. infantum* hinge carries pLDDT of 60.3 to 90.9, so the comparison inherits that uncertainty. Side-chain atoms from neighbouring regions approach more closely than the backbone does. This analysis was added at revision and was not pre-registered. Every value is a live formula computed from the 'Per-residue distances' sheet.

Core baseline, residues 52 to 425

Human model	Residues	Core Ca pairs fitted	Core RMSD (Å)	Median distance (Å)	90th percentile	95th percentile
ENTPD1	510	273	1.14	0.94	2.97	3.68
ENTPD2	495	246	1.42	1.34	3.30	4.13
ENTPD3	529	255	1.15	1.03	3.18	4.00
ENTPD4	616	209	1.80	1.96	3.38	4.00
ENTPD5	428	258	0.94	0.83	3.50	4.57
ENTPD8	495	268	1.37	1.32	3.01	4.16

Pooled 95th percentile of the core distribution (Å) **4.10**

Hinge, residue by residue

Residue	Substituted	ENTPD1	ENTPD2	ENTPD3	ENTPD4	ENTPD5	ENTPD8	Smallest	Backbone equivalent?
P40	yes	7.02	8.60	7.90	5.84	8.69	7.92	5.84	none
L41		7.66	8.23	8.80	6.48	8.56	9.05	6.48	none
L42		6.61	6.25	6.97	5.99	7.00	6.55	5.99	none
S43	yes	6.11	5.28	6.65	5.47	6.77	5.65	5.28	none
P44	yes	6.43	5.85	6.66	4.22	6.76	5.64	4.22	none
C45		5.62	4.97	5.83	4.92	6.00	5.40	4.92	none
D46		7.51	7.14	7.09	7.60	7.65	6.64	6.64	none
S47		5.04	5.07	3.46	5.67	5.00	4.05	3.46	yes
A48		3.93	3.85	2.85	5.33	4.60	3.74	2.85	yes
Y49	yes	2.47	1.70	1.93	3.10	1.92	0.57	0.57	yes
A50		1.40	1.26	1.66	2.09	1.50	1.08	1.08	yes
N51		1.20	0.70	0.41	1.45	0.75	1.15	0.41	yes

Table S17. The terminal-free hinge axis through equilibration and production. The axis is the angle at the centroid of Calpha 40 to 42, between the centroid of Calpha 49 to 51 and the centroid of the catalytic core, as defined in Section 2. Mutant systems were built by side-chain substitution on wild-type coordinates, so both genotypes of a species begin production from the same backbone. The predicted mutant models were not used, and their axis values are given at the foot of the table for reference only. The first two stages therefore test whether the genotypes differ before the dynamics have run. Inference is at the level of the trajectory, by Welch t test on the ten replicate means per arm, with Holm correction across the five stages within each species. The 0 to 5 ns window is normally discarded and is included here only to show the approach to the production windows. This analysis was added at revision and was not pre-registered. Every value is a live formula computed from the 'Per-replicate data' sheet.

Species	Stage	Wild type mean	Wild type SD	Hinge mutant mean	Hinge mutant SD	Difference	Hedges' g	p	Holm p
L. infantum									
L. infantum	First production frame	36.35	3.81	40.18	3.02	+3.84	+1.07	0.0231	0.0693
L. infantum	First 1 ns	40.12	4.61	41.52	4.85	+1.40	+0.28	0.5174	0.5174
L. infantum	0 to 5 ns	38.74	4.96	43.91	6.05	+5.17	+0.90	0.0516	0.1032
L. infantum	5 to 30 ns	32.07	5.12	45.19	4.56	+13.12	+2.59	<0.0001	0.0001
L. infantum	30 to 55 ns	29.08	6.26	43.42	7.59	+14.34	+1.97	0.0002	0.0010
L. major									
L. major	First production frame	46.72	5.87	49.68	4.58	+2.96	+0.54	0.2255	0.2255
L. major	First 1 ns	44.58	6.46	48.97	3.62	+4.39	+0.80	0.0814	0.2175
L. major	0 to 5 ns	40.37	6.02	46.26	7.65	+5.89	+0.82	0.0725	0.2175
L. major	5 to 30 ns	36.29	3.68	44.00	10.71	+7.71	+0.92	0.0541	0.2165
L. major	30 to 55 ns	32.56	10.05	46.47	11.38	+13.91	+1.24	0.0097	0.0485

Predicted models, for reference. Not used as starting structures.

L. infantum	Wild type	36.25	AlphaFold predicted model (deg)
L. infantum	Hinge mutant	49.04	AlphaFold predicted model (deg)
L. major	Wild type	46.47	AlphaFold predicted model (deg)
L. major	Hinge mutant	47.69	AlphaFold predicted model (deg)

Table S18. Relaxation of the Arg324 backbone during simulation. The predicted models place Arg324 at positive phi with strongly negative psi in both *L. infantum* structures, a combination that is sterically disallowed, while both *L. major* structures place it in right-handed alpha. Backbone dihedrals were measured on every frame of all forty replicates and summarised with circular statistics, since phi and psi cannot be averaged linearly. A replicate is counted as strained where its circular mean phi is positive and its circular mean psi is below -30 degrees, which is the region the models started in. Left-handed alpha, at phi near +60 and psi near +40, is a populated and allowed region and is counted as relaxed. The 0 to 5 ns window is normally discarded and is included here to show when the relaxation occurs. This analysis was added at revision and was not pre-registered. Every value is a live formula computed from the 'Per-replicate data' sheet.

Species	Genotype	Window	Right-handed alpha	Left-handed alpha	Positive phi	Replicates in right-handed alpha	Replicates in left-handed alpha	Replicates still strained
L. infantum	Wild type	0 to 5 ns	0.554	0.239	0.443	6	4	0
L. infantum	Wild type	5 to 30 ns	0.642	0.265	0.356	7	3	0
L. infantum	Wild type	30 to 55 ns	0.590	0.261	0.409	6	3	1
L. infantum	Hinge mutant	0 to 5 ns	0.186	0.395	0.814	2	6	2
L. infantum	Hinge mutant	5 to 30 ns	0.556	0.319	0.443	6	4	0
L. infantum	Hinge mutant	30 to 55 ns	0.599	0.296	0.400	6	4	0
L. major	Wild type	0 to 5 ns	0.998	0.000	0.001	10	0	0
L. major	Wild type	5 to 30 ns	0.957	0.022	0.041	10	0	0
L. major	Wild type	30 to 55 ns	0.999	0.000	0.000	10	0	0
L. major	Hinge mutant	0 to 5 ns	0.998	0.000	0.000	10	0	0
L. major	Hinge mutant	5 to 30 ns	0.991	0.002	0.008	10	0	0
L. major	Hinge mutant	30 to 55 ns	0.998	0.000	0.000	10	0	0

Predicted models, dihedrals at Arg324

Model	phi (deg)	psi (deg)	Region
L. infantum wild type	+61.6	-20.3	positive phi, disallowed
L. infantum hinge mutant	+27.6	-19.3	positive phi, disallowed
L. major wild type	-48.9	-11.2	right-handed alpha
L. major hinge mutant	-49.8	-14.8	right-handed alpha

Table S19. Thermostat and barostat diagnostics across production, and the solute/solvent temperature split. Temperature, potential energy and box volume were recorded every 20 ps throughout production for all forty replicates, giving 2750 points per trajectory. Density is the fixed system mass divided by the instantaneous box volume. Slopes are ordinary least squares fits of the quantity against time within each replicate, so they measure drift across the 55 ns of production. The first block addresses thermostat stability, the second barostat convergence, and the third the partition of kinetic energy between solute and solvent. For the third block, the forty saved simulation states that carry velocities, one per replicate at the end of production, were each assigned a subsystem temperature from T = 2E_kin/(N_dof k_B), with degrees of freedom counted from the simulation system itself so that rigid water contributes six per molecule, constrained hydrogen bonds are subtracted and the repartitioned hydrogen masses are the ones used. As a validation, the whole-system temperature recomputed this way reproduces the logged value at every one of the forty timesteps to 0.0000 K. Equipartition predicts an instantaneous standard deviation of T*sqrt(2/N_dof), which is 3.57 K for the solute at 15,086 degrees of freedom and 1.34 K for the solvent at 107,235, hence 3.81 K for their difference against 3.35 K observed. Total energy is not tabulated because it is not a conserved quantity in the constant-pressure, constant-temperature ensemble simulated here, where both the Langevin thermostat and the Monte Carlo barostat exchange energy with the system by construction. Every value is a live formula computed from the two data sheets. The thermostat setpoint was 310.0 K, and mean production temperatures of 310.99 to 311.00 K correspond to a constant offset of approximately +1.0 K, or 0.32 per cent, present with the same sign and magnitude in all forty replicates. This is the discretisation error expected of a Langevin integrator at a 4 fs timestep with hydrogen mass repartitioning, and the slopes tabulated here show no systematic drift across production. The means are therefore not expected to agree exactly with the setpoint.

Thermostat, setpoint 310.0 K

Species	Genotype	Mean T (K)	Offset from setpoint (K)	SD of T (K)	Lowest T (K)	Highest T (K)	Mean slope (K/ns)	Drift over 55 ns (K)	Replicates with p < 0.05
L. infantum	Wild type	310.992	+0.992	1.267	305.982	316.392	-0.00029	-0.016	0
L. infantum	Hinge mutant	311.001	+1.001	1.258	305.924	315.821	+0.00031	+0.017	0
L. major	Wild type	310.989	+0.989	1.351	305.818	316.650	+0.00037	+0.020	0
L. major	Hinge mutant	311.001	+1.001	1.349	305.913	316.389	-0.00061	-0.033	1

Barostat

Species	Genotype	Volume, first frame (nm3)	Mean volume (nm3)	SD of volume (nm3)	First frame minus mean, in SD	Mean slope (nm3/ns)	Drift over 55 ns (nm3)	Mean density (g/cm3)	Replicates with p < 0.05
L. infantum	Wild type	592.421	592.260	1.022	+0.16	-0.00256	-0.141	1.0296	8
L. infantum	Hinge mutant	596.146	595.774	1.026	+0.36	-0.00131	-0.072	1.0293	4
L. major	Wild type	510.462	510.379	0.942	+0.09	-0.00038	-0.021	1.0347	2
L. major	Hinge mutant	510.675	510.850	0.950	-0.18	-0.00149	-0.082	1.0345	2

Solute and solvent temperature, end of production, one snapshot per replicate

Species	Genotype	Replicates	Solute T (K)	Solvent T (K)	Solute minus solvent (K)	SD of difference (K)	SE of difference (K)	t against zero	p (two sided)
L. infantum	Wild type	10	312.640	311.427	+1.213	4.297	1.359	+0.893	0.395
L. infantum	Hinge mutant	10	311.819	310.832	+0.987	1.658	0.524	+1.882	0.092
L. major	Wild type	10	311.254	310.617	+0.637	3.755	1.187	+0.537	0.605
L. major	Hinge mutant	10	311.758	311.111	+0.647	3.613	1.143	+0.566	0.585
All arms pooled		40	311.868	310.997	+0.871	3.350	0.530	+1.644	0.108

Validation, computed whole-system T minus logged T (K)	0.0000	0.0000	0.0000	largest absolute

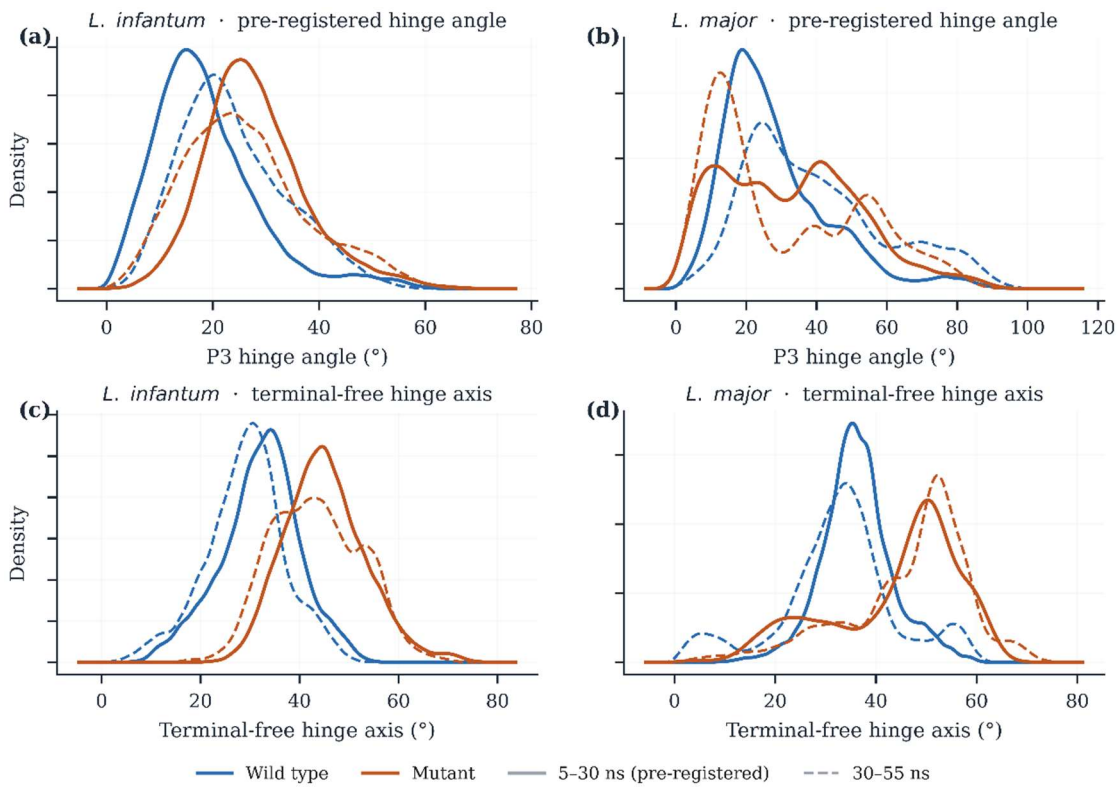


Figure S6. Pooled conformational distributions of the two hinge measures in each analysis window. Density is estimated from all frames pooled across the ten replicates of each arm, so the comparison is of the conformational range sampled rather than of the window means. Wild type in blue, hinge mutant in orange, the pre-registered 5 to 30 ns window as a solid line and the 30 to 55 ns window as a dashed line. (a,b) The pre-registered hinge angle. In *L. infantum* the genotypes separate in the primary window and the two distributions converge in the second, which is the distributional form of the decline from +9.35 to +2.11 degrees between windows. In *L. major* the measure is broad and multimodal in both windows and the genotypes overlap throughout, consistent with the 18.3 degree detection limit on that comparison. (c,d) The terminal-free hinge axis. In *L. infantum* the separation is present in both windows and each genotype samples the same range in each. In *L. major* the separation is present but the distributions are less regular. This figure shows frame-level sampling only. All inference is at the level of the trajectory, and the per-replicate values on which it rests are shown in Supplementary Figure S8 and tabulated in Table S20.

Table S20. Per-replicate values underlying Supplementary Figure S8. Each trajectory contributes one value per metric, obtained by averaging that metric across all frames of the primary 5 to 30 ns analysis window within that replicate, giving ten independent values per arm. The within-replicate standard deviation is the spread of the per-frame values inside a single trajectory and is plotted in Supplementary Figure S8 as the thin vertical line behind each point. It describes conformational sampling within one trajectory and is not an uncertainty on the replicate mean. The pre-registered hinge angle is the angular displacement of the Ca40 to Ca51 vector from its orientation in the wild-type starting structure of the same species, measured after superposition on the catalytic core, with a single common reference used for both genotypes. The terminal-free axis is the angle at the centroid of Ca40 to 42 between the centroid of Ca49 to 51 and the centroid of the catalytic core and is invariant to superposition. Genotypes are compared by a two-tailed Welch t test on the ten replicate means, with Hedges' g corrected for small samples. Replicates, not frames, are the unit of replication. Values were calculated from the underlying per-replicate data.

Pre-registered hinge angle

Species	Replicates per arm	Wild type, mean (deg)	Wild type, SD (deg)	Mutant, mean (deg)	Mutant, SD (deg)	Difference (deg)	SE of difference (deg)	Welch p	Hedges' g
L. infantum	10	18.659	5.854	28.004	5.151	+9.345	2.466	0.0014	+1.62
L. major	10	28.346	12.871	33.131	14.688	+4.786	6.176	0.4486	+0.33

Terminal-free hinge axis

Species	Replicates per arm	Wild type, mean (deg)	Wild type, SD (deg)	Mutant, mean (deg)	Mutant, SD (deg)	Difference (deg)	SE of difference (deg)	Welch p	Hedges' g
L. infantum	10	32.069	5.117	45.190	4.563	+13.122	2.168	<0.0001	+2.59
L. major	10	36.293	3.676	43.997	10.710	+7.704	3.581	0.0543	+0.92

Table S21. Cross-validation of the helix assignment at residues 40 to 43 by a method that does not use hydrogen bonds. DSSP assigns secondary structure from an electrostatic hydrogen-bond energy criterion. The geometric assignment applies the P-SEA criteria, which use only the positions of alpha carbons, through three interatomic distances and two angles, so no hydrogen bond enters the calculation at any point. A frame is counted as helical if any residue from 40 to 43 is assigned helix by the method in question. Both assignments were computed on the same 2500 frames of each replicate across the full 5 to 55 ns production period, giving 100,000 frames in total. Before use, the geometric implementation was validated against DSSP on the wild-type starting structure, where it reproduced the DSSP assignment across all 390 residues with 90.8 per cent agreement and a Jaccard index of 0.762 on helical residues, being slightly more conservative at helix termini as expected of that method. These two figures have different denominators. Percentage agreement is taken over all 390 residues and therefore includes the large majority that both methods assign as non-helical. The Jaccard index is taken over helical assignments only, as the number of residues assigned helix by both methods divided by the number assigned helix by either, and so excludes residues that both methods call non-helical. It is accordingly the stricter of the two measures. Percentages in the lower table are pooled across the ten replicates of each arm, weighted by frame count. Cohen's kappa measures frame-by-frame concordance between the two assignments. The correlation is between the ten per-replicate occupancies given by each method, which is the quantity on which the manuscript performs inference.

Helix occupancy at residues 40 to 43, pooled across ten replicates per arm

Species	Genotype	Frames	DSSP helix (%)	Geometric helix (%)	Frames helical by both	DSSP frames confirmed geometrically (%)	Cohen's kappa	Correlation of replicate occupancies	DSSP median episode (ps)
L. infantum	Wild type	25,000	0.000	1.440	0	n/a	n/a	undefined, DSSP zero in all ten	0.0
L. infantum	Hinge mutant	25,000	28.012	25.132	3,948	56.4	0.448	0.9813	20.0
L. major	Wild type	25,000	0.000	0.052	0	n/a	n/a	undefined, DSSP zero in all ten	0.0
L. major	Hinge mutant	25,000	0.976	1.772	169	69.3	0.486	0.9920	0.0

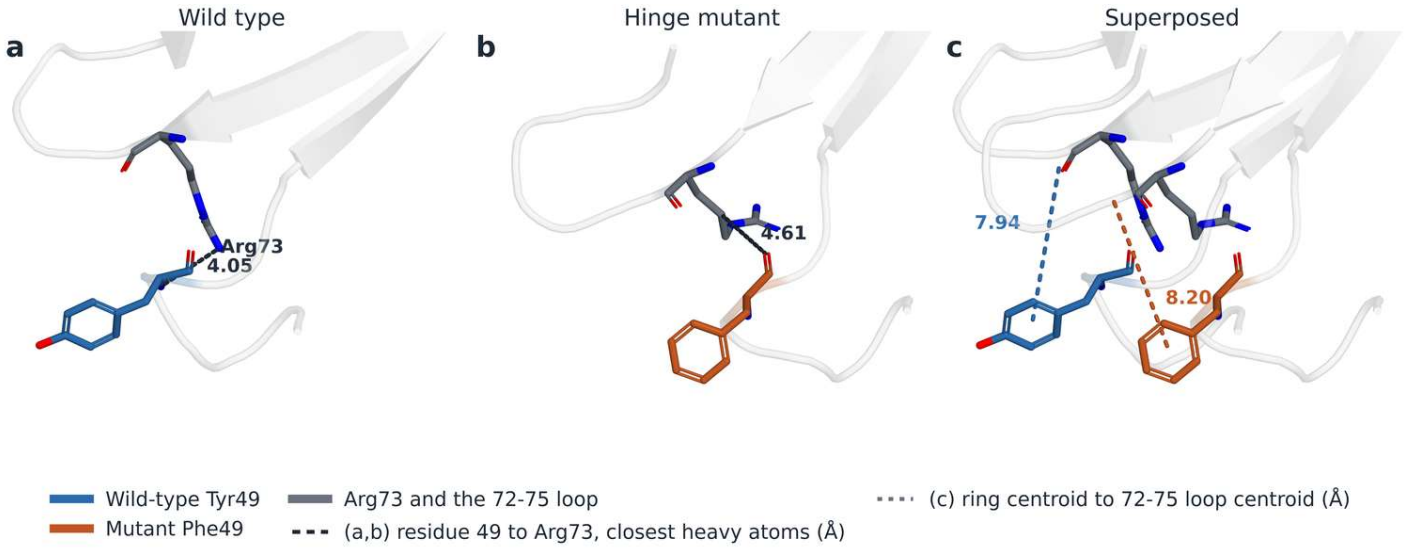


Figure S7. Representative structures of the residue 49 to Arg73 cluster in *L. infantum*. (a) Wild type, (b) hinge mutant, and (c) the two superposed on the catalytic core, residues 52 to 425, so that all three panels share one frame of reference. Frames were selected by a fixed rule rather than by inspection: within each arm, the replicate whose median residue 49 to Arg73 closest heavy-atom distance lay nearest that arm's median was taken, and within that replicate the frame nearest its own median. Both arms returned replicate 8, giving wild-type frame 2456 at 54.12 ns and mutant frame 210 at 9.20 ns. Residue 49 is drawn as sticks and coloured by genotype, wild-type Tyr49 in blue and mutant Phe49 in orange. Arg73 and the 72 to 75 loop are the fixed reference against which displacement is measured and are grey in both, with the surrounding backbone as a transparent ribbon. Dashed lines in (a) and (b) connect the closest pair of heavy atoms between residue 49 and Arg73, 4.05 Å in the wild type and 4.61 Å in the mutant, against arm medians of 4.03 and 4.65 Å. Because this is a minimum over all atom pairs, the endpoints are not necessarily the same two atoms in both panels, and restricting the comparison to heavy atoms present in both genotypes gives identical occupancies, so the difference does not arise from the mutant having one fewer heavy atom at this position. Dashed lines in (c) mark a different quantity, the distance from the aromatic ring centroid to the centroid of the whole 72 to 75 loop, 7.94 Å in the wild type and 8.20 Å in the mutant. This is necessarily longer than the distances in (a) and (b) because both endpoints are averaged positions. The displacement is sub-ångström in both measures and typical of the ensemble rather than an extreme case. Across all ten replicates per arm the residue 49 to Arg73 median distance rises by 0.62 Å ($p = 0.0017$, $g = +1.64$) and the ring moves 0.71 Å further from the loop ($p = 0.062$, $g = +0.85$). Because occupancy in Table 8 is scored at 4.0, 4.5 and 5.0 Å cutoffs, this sub-ångström displacement is sufficient to produce the large occupancy changes reported there.

Table S22. Geometry of the residue 49 to Arg73 cluster and hydrogen bonding of the Tyr49 hydroxyl in *L. infantum*. All values are computed from the full 5 to 55 ns analysis window of every replicate, 2500 frames each and 25,000 frames per arm. Distances are medians within a replicate, so each arm contributes ten independent values, and genotype comparisons are two-tailed Welch t tests on those ten values, with Hedges' g corrected for small samples. The ring is the six aromatic carbons of residue 49, Tyr in the wild type and Phe in the mutant. A hydrogen bond was counted when the hydrogen to acceptor distance fell below 2.5 Å and the donor to hydrogen to acceptor angle exceeded 120 degrees, with the hydroxyl treated as donor and as acceptor in turn. Production trajectories retain protein coordinates only, so hydrogen bonds to water cannot be assessed and no claim is made about them. The lower block lists every protein partner of the Tyr49 hydroxyl, pooled across the ten wild-type replicates. Arg73 itself appears in four frames of 25,000, which is why the loss of the hydroxyl does not account for the change in contact occupancy reported in Table 8.

Cluster geometry, medians across ten replicates per arm

Measure	Wild type, mean (Å)	Wild type, SD	Mutant, mean (Å)	Mutant, SD	Difference (Å)	Welch p	Hedges' g	Replicates per arm
Residue 49 to Arg73, closest heavy atom	4.029	0.266	4.653	0.443	+0.624	0.0017	+1.64	10
Ring to 72-75 loop, closest heavy atom	5.611	0.783	6.321	0.809	+0.710	0.0615	+0.85	10
Ring centroid to loop centroid	8.286	1.017	9.175	1.223	+0.890	0.0944	+0.76	10

Protein hydrogen-bonding partners of the Tyr49 hydroxyl, wild type, 25,000 frames

Partner residue	Role of the hydroxyl	Frames	Occupancy (%)
Gln38	donor and acceptor	502	2.008
Arg75	acceptor	216	0.864
Glu72	donor	25	0.100
Tyr36	donor and acceptor	15	0.060
Tyr37	donor and acceptor	8	0.032
Arg73	donor and acceptor	4	0.016
Leu41	donor	3	0.012
Ser39	acceptor	2	0.008
Gly74	donor	1	0.004
Any protein partner	one or more of the above	747	2.988
No protein partner	hydroxyl free of any protein contact	24,253	97.012

Residue occupancies sum to slightly more than the "any partner" row because a few frames carry two partners at once.

Table S23. Terminal-free axis difference between genotypes in consecutive 5 ns bins across the whole production period. Because both arms begin from identical coordinates the difference is zero at the start of production. Differences are mutant minus wild type in degrees, with the p value from a two-tailed Welch test on ten per-replicate values in each bin. The slope of the difference in the final row is fitted to the per-replicate axis angles rather than to the ten bin means, so that between-replicate variance is retained, and the unit of inference remains the trajectory.

Bin (ns)	*L. infantum* difference	*L. infantum* p	*L. major* difference	*L. major* p
5 to 10	+11.65	0.0002	+10.90	0.0266
10 to 15	+15.55	<0.0001	+7.74	0.0766
15 to 20	+14.13	0.0012	+8.09	0.0734
20 to 25	+12.52	0.0013	+6.25	0.1548
25 to 30	+11.75	0.0027	+5.56	0.2616
30 to 35	+13.52	0.0011	+8.89	0.0846
35 to 40	+14.52	0.0005	+14.69	0.0237
40 to 45	+14.46	0.0004	+14.36	0.0067
45 to 50	+13.47	0.0023	+14.98	0.0054
50 to 55	+15.73	0.0001	+16.65	0.0055
Slope of the difference (deg ns^{-1})	+0.039	0.6284	+0.193	0.1876

In L. infantum the difference is established within the first 5 ns of analysed production, is significant in every bin, and shows no trend. In *L. major* the slope of the difference is positive but does not reach significance. The pattern reflects the wild-type arm continuing to relax, from approximately 36 degrees across the first 30 ns to 30.1 degrees in the final bin, while the mutant arm remains between 41.6 and 47.2 degrees. Neither arm's slope differs from zero at replicate level. Fitting the slope to the ten bin means instead gives +0.0383 and +0.1968 at p = 0.2460 and 0.0155, but ten bins drawn from the same twenty trajectories are not ten independent observations, so those values are reported only for comparison. Both hinge measures are shown per replicate in Supplementary Figure S8, with each trajectory contributing a single point. The pooled conformational distributions in each window are shown in Supplementary Figure S6.

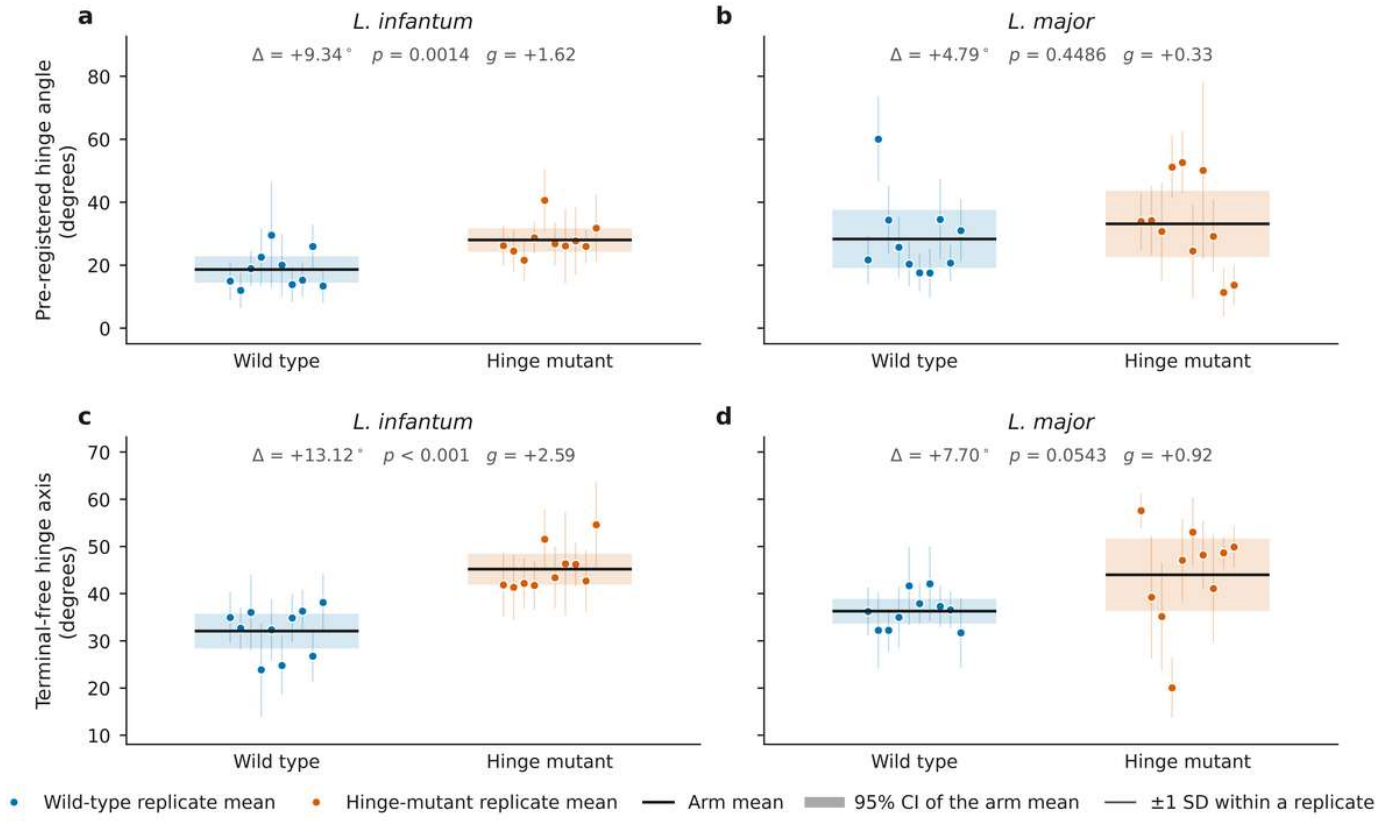


Figure S8. Hinge geometry at the level of the independent trajectory, primary 5 to 30 ns window. (a,b) Pre-registered hinge angle and (c,d) terminal-free hinge axis, for *L. infantum* (a,c) and *L. major* (b,d). Each filled circle is the mean of one replicate across that window, so each panel shows ten independent trajectories per genotype. Wild type in blue, hinge mutant in orange. The thin vertical line behind each circle spans ±1 standard deviation of the per-frame values within that replicate and describes conformational sampling inside a single trajectory, not uncertainty on the replicate mean. The horizontal rule is the arm mean and the shaded band is its 95% confidence interval across the ten replicates. Reported above each panel are the genotype difference, the p value from a two-tailed Welch t test on the ten replicate means, and Hedges' g with the small-sample correction. In (c) every mutant replicate exceeds every wild-type replicate. Replicates, not frames, are the unit of replication throughout, and the per-replicate values are given in Table S20.

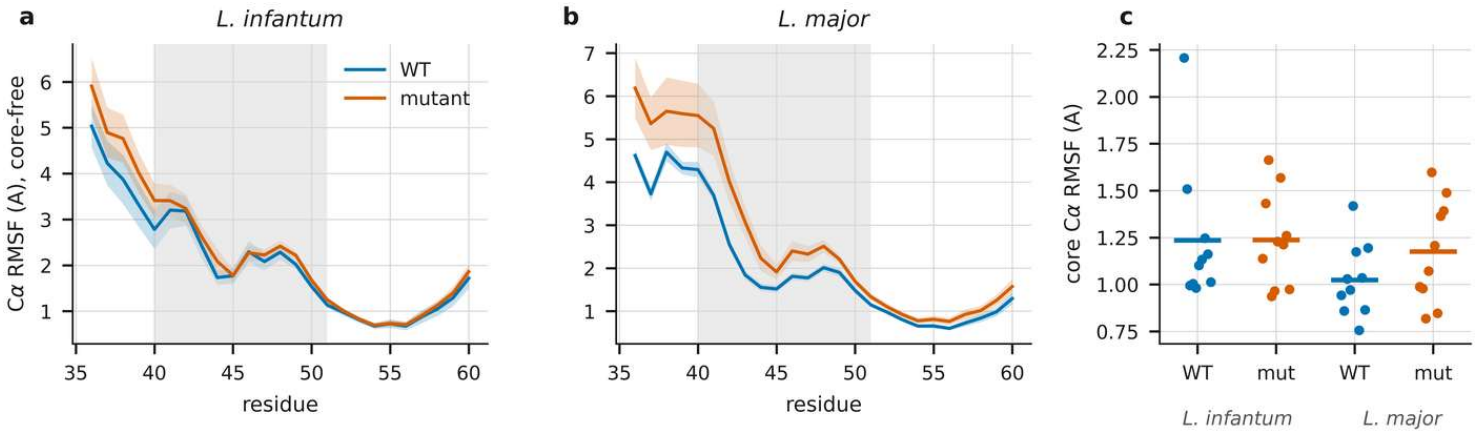


Figure S9. Backbone fluctuation. (a,b) Per-residue Cα root-mean-square fluctuation across residues 36 to 60, computed without superposition on this region so that motion of the catalytic core cannot propagate into it, in (a) *L. infantum* and (b) *L. major*. Wild type in blue, hinge mutant in orange, with the shaded band showing the standard error across the ten replicates of each genotype. The grey vertical span marks the hinge, residues 40 to 51. Fluctuation is higher in the mutant at every residue from 36 to 45 in both species and converges between genotypes beyond residue 51. The statistical comparison was made on the mean across residues 36 to 45 as a single value per replicate, and the per-residue profile is shown as descriptive localisation. In a construct lacking the transmembrane segment these residues form a free terminus, so the quantity is not equivalent to mobility of that region in the intact protein. (c) Core Cα root-mean-square fluctuation, residues 52 to 425, as one value per replicate in each of the four systems, with the horizontal bar showing the mean across ten replicates. This comparison is null in both species.